

Article

# The Microstructure and Mechanical Properties of Die-Cast Mg-6Al-2Sm-*x*Cu Alloys

Jiaan Liu \*, Chunxue Yang and Mengli Yang

Key Laboratory of Automobile Materials (Ministry of Education), College of Materials Science and Engineering, Jilin University, Changchun 130022, China; yangcx15@mails.jlu.edu.cn (C.Y.); yangml16@mails.jlu.edu.cn (M.Y.)

\* Correspondence: liuja@jlu.edu.cn; Tel.: +86-431-8509-5862

Academic Editor: Daolun Chen

Received: 8 March 2017; Accepted: 5 May 2017; Published: 10 May 2017

**Abstract:** In the present study, the effect of Cu content on the microstructure and mechanical properties of die-cast Mg-6Al-2Sm-*x*Cu (*x* = 1, 3, 5) alloys has been investigated. The microstructure and components of the alloys were observed and identified by optical microscopy (OM), scanning electron microscopy (SEM), transmission electron microscopy (TEM), and energy dispersive spectroscopy (EDS), respectively. The phases of the alloys were analyzed via X-ray diffractometer (XRD). The mechanical properties at different temperatures were studied by tensile tests. The experimental results show that all die-cast Mg-6Al-2Sm-*x*Cu alloys consist of  $\alpha$ -Mg,  $\beta$ -Mg<sub>17</sub>Al<sub>12</sub>, Al<sub>4</sub>Cu<sub>9</sub>, Al<sub>3</sub>Sm, and Mg<sub>2</sub>Cu<sub>6</sub>Al<sub>5</sub> phases. These components, i.e., Al<sub>3</sub>Sm and Al<sub>4</sub>Cu<sub>9</sub> phases, have high thermal stability and can prohibit dislocation movement and grain boundary sliding. TEM analysis shows that the Al<sub>3</sub>Sm phase possesses a tetragonal structure. With the increase in Cu content, the microstructure is refined firstly and then becomes coarsened. Moreover, the tensile strength increases firstly and then decreases as Cu content increases at room temperature and an elevated temperature. All fractures of the alloys at room temperature show a complex mode of brittle and ductile fracture. However, at an elevated testing temperature, the fractures of the alloys exhibit more ductile fractures.

**Keywords:** Cu content; microstructure; mechanical properties; die-cast Mg-6Al-2Sm-*x*Cu alloys

## 1. Introduction

The density of magnesium is 1.78 g/cm<sup>3</sup>, which is 2/3 the density of aluminum and is 1/4 the density of steel [1,2], so magnesium alloys are the lightest metallic structural materials [3–6]. Besides that, magnesium alloys possess high specific strength and specific stiffness, good shock absorption capability and workability, excellent shielding and thermal conductivity, replicability, etc. [7–12]. However, when the temperature used is higher than 120 °C, applications of these alloys are limited due to their poor creep resistance and large decrease in strength at elevated temperatures [13–20]. The weak properties of magnesium alloys, such as the low absolute strength and the poor heat-resistance, seriously hinder their wide applications [3,21]. Therefore, it is of great importance to design and develop magnesium alloys with high comprehensive mechanical properties, including high strength and heat resistance.

Rare earth (RE) elements have been proven as an effective approach to improve the comprehensive performance of Mg-Al-based alloys [6,9,13]. Recently, investigations have been performed on Mg-Al-based alloys with RE elements (i.e., Sm). Samarium is one of the lighter RE elements belonging to the cerium group, with a maximum solubility in solid Mg of 5.8 wt. % at a eutectic temperature of 803 K [13]. Compared with other RE elements, the effects of cheaper Sm on the microstructure and mechanical properties of Mg-Al series alloys have rarely been studied [4,22]. Zheng [23,24] reported the microstructure, mechanical properties, and creep behavior of a Mg-3Sm-0.5Zn-0.4Zr (wt. %) alloy. The ultimate tensile strength (UTS), yield strength (YS), and elongation  $\delta$  were 189 MPa, 94 MPa,

and 11.7%, respectively. Moreover, Huang *et al.* [25] reported that the microstructure of an as-cast Mg-6.02Al-1.03Sm alloy was composed of  $\alpha$ -Mg matrix, a discontinuous  $\beta$ -Mg<sub>17</sub>Al<sub>12</sub> phase, and a small block Al<sub>2</sub>Sm phase, and the as-cast alloys exhibited excellent tensile mechanical properties. The tensile strength ( $\sigma_b$ ) and elongation rate ( $\delta$ ) reached 205–235 MPa and 8.5–16.0% at ambient temperature, respectively. Meanwhile, they also exceeded 160 MPa and 14.0% at 423 K, respectively.

Cu is commonly used to improve the heat resistance of Mg–Al-based alloys. Researchers have reported that the addition of Cu significantly improved the creep resistance of Mg–Al alloys. However, to date, the research on die-cast Mg-6Al-2Sm-*x*Cu alloys is scarce. Therefore, in this study, the microstructure and mechanical properties of die-cast Mg-6Al-2Sm-*x*Cu alloys were investigated, *i.e.*, the effect of Cu content on the microstructure and strength of the alloys.

## 2. Materials and Methods

The experimental alloys are die-cast Mg-6Al-2Sm-*x*Cu alloys with 1 wt. %, 3 wt. %, and 5 wt. % Cu. Industrial pure magnesium (99.5%), pure aluminum (99.5%), Al-Be, Al-10% Mn, Al-40% Sm master alloys, and added Cu were adopted into the alloys in the form of Al-50% Cu master alloys. The melting of the experimental alloys was carried out in an MRL-8 magnesium alloy melting furnace, and RJ-6 was selected as the covering agent and the refining agent, which consists of MgCl<sub>2</sub> (35%), KCl (27%), NaCl (26%), CaCl<sub>2</sub> (8%), MgO (1.25%), H<sub>2</sub>O (1.5%), and undissolved substance (1.25%). The electric resistance furnace was filled with protective gases CO<sub>2</sub> and SF<sub>6</sub>. The pressure casting was carried out using an E53D horizontal cold chamber die casting machine at 60 MPa for a holding time of 12 s.

The magnesium alloy samples were ground and polished, and then were etched in a 4% nitric acid alcohol solution.

The microstructure and composition of the alloys were analyzed via optical microscopy (OM, MDJ-DM320, HIE Co. Ltd., Zhengzhou, China), scanning electron microscopy (SEM, JXA-8100, JEOL, Tokyo, Japan) with energy dispersive spectroscopy (EDS, OXFORD 7412, PI Co. Ltd., Shanghai, China), and transmission electron microscopy (TEM, JEM-1230, JEOL, Tokyo, Japan). The grain size was measured by Nano Measurer 1.2, with more than 100 grain sizes on the metallographic image, and the average value was used as the final grain size. The phase structure was analyzed via an X-ray diffractometer (XRD, DMAX-RB 12KW, Rigaku, Beijing, China) with Cu K $\alpha$  radiation.

The tensile samples were cut from the bottom of a cylinder ingot using an electric-spark wire-cutting machine. The gage dimensions of the tensile specimen were 15 × 3.5 × 1.5 mm<sup>3</sup>. The axial tension tests at room temperature and 150 °C were carried out on the MTS-810 material testing machine (MTS System Corporation, Minneapolis, MN America) and the INSTRON-5869 universal testing machine (ITET Co. Ltd., Shanghai, China), respectively. Moreover, the strain rate was 7.5 × 10<sup>−4</sup> s<sup>−1</sup>. The value of the tensile test in the study was the average of at least three measurements. The tensile samples at 150 °C were held for about 10 min to keep testing temperature.

The fractures of the samples were observed by SEM after the tensile tests.

## 3. Results and Discussion

### 3.1. Microstructure of Die-Cast Mg-6Al-2Sm-*x*Cu Alloys (*x* = 1, 3, 5)

Figure 1 shows the optical images of the microstructure of the die-cast Mg-6Al-2Sm-*x*Cu (*x* = 1, 3, 5) alloys. Figure 1a–c are taken from the same zone of the samples. It can be seen that the grain size increases firstly and then decreases when the Cu content increases from 1 to 5%. The mean grain sizes of the three alloys are 16.35  $\mu$ m, 9.88  $\mu$ m, and 13.19  $\mu$ m, respectively. When the Cu content is 3%, the grain size is finest among the three alloys. The grain size of the Mg-6Al-2Sm-5Cu alloy is coarser than that of the Mg-6Al-2Sm-3Cu alloy, but is still finer than that of the Mg-6Al-2Sm-1Cu alloy. Moreover, with the increase in Cu content, the coarse columnar grain tends to be a fine equiaxed grain. It can be seen that, when Cu content is 3%, the alloy exhibits the most homogeneous microstructure.

Therefore, it can be inferred that the alloy containing 3% Cu presents excellent mechanical properties among the three alloys.

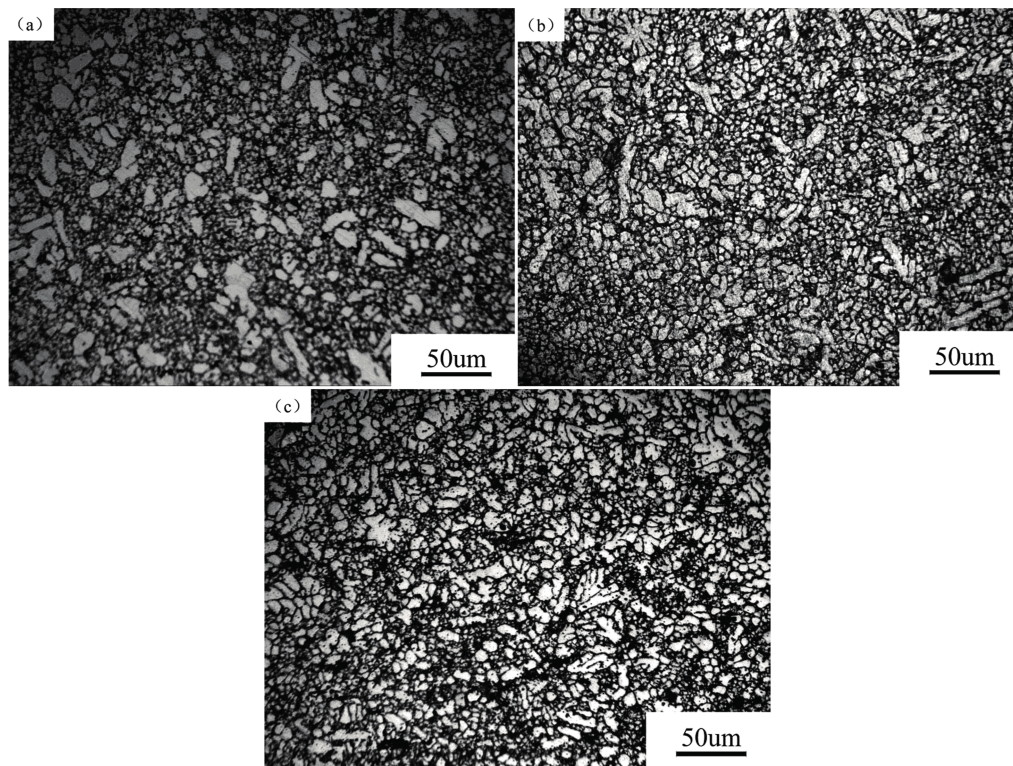


**Figure 1.** Optical images of the microstructure of the die-cast alloys: (a) Mg-6Al-2Sm-1Cu; (b) Mg-6Al-2Sm-3Cu; (c) Mg-6Al-2Sm-5Cu.

Figure 2 shows the XRD patterns of the three alloys. It can be seen that all alloys consist of  $\alpha$ -Mg matrix,  $\beta$ -Mg<sub>17</sub>Al<sub>12</sub>, Al<sub>4</sub>Cu<sub>9</sub>, Al<sub>3</sub>Sm, and Mg<sub>2</sub>Cu<sub>6</sub>Al<sub>5</sub>.

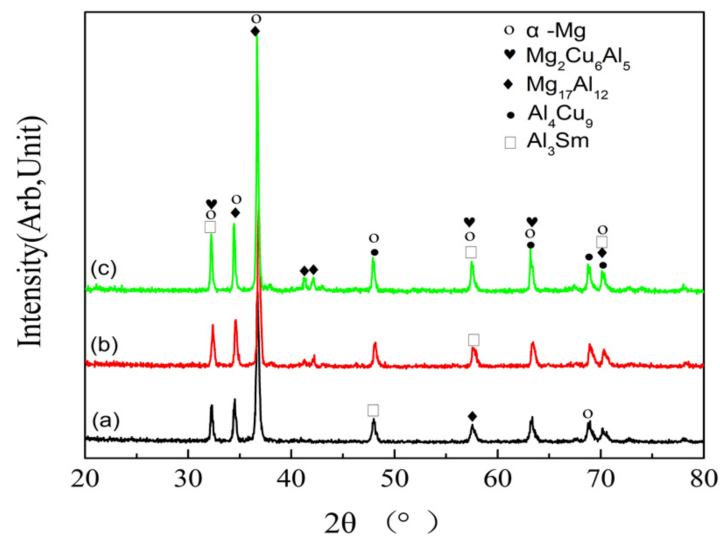


**Figure 2.** XRD patterns of the die-cast alloys: (a) Mg-6Al-2Sm-1Cu; (b) Mg-6Al-2Sm-3Cu; (c) Mg-6Al-2Sm-5Cu.

Figure 3 shows the SEM morphologies and EDS results of all kinds of phases of the die-cast alloys. Combining the XRD analysis results, the phases, including  $\alpha$ -Mg,  $\beta$ -Mg<sub>17</sub>Al<sub>12</sub>, Al<sub>4</sub>Cu<sub>9</sub>, Al<sub>3</sub>Sm, and Mg<sub>2</sub>Cu<sub>6</sub>Al<sub>5</sub>, are marked in the SEM image. The gray region is the  $\alpha$ -Mg matrix. The bulk bone-like phase that distributes along the grain boundary is  $\beta$ -Mg<sub>17</sub>Al<sub>12</sub>. The point-like phase is the Al<sub>4</sub>Cu<sub>9</sub> phase. The long strip shape of the phase is the Mg<sub>2</sub>Cu<sub>6</sub>Al<sub>5</sub> phase. Moreover, the small block phase is the Al<sub>3</sub>Sm phase. Mn is shown in the EDS result because Mn exists in the master alloy (Al-10% Mn). The content of Mn is a small amount; therefore, Mn cannot be taken as the main alloying element.

SEM morphologies and EDS results of the net structure of all die-cast alloys are shown in Figure 4a,d,g and Figure 4c,f,i, respectively. Moreover, Figure 4b,e,h are the corresponding local enlarged regions of Figure 4a,d,g. The  $\alpha$ -Mg matrix has little effect on the improvement of alloy strength. The bulk bone-like  $\beta$ -Mg<sub>17</sub>Al<sub>12</sub> phase clearly distributes along the grain boundary. The preliminary observation shows that, with the increase in Cu content, the discontinuous bulk bone-like  $\beta$ -Mg<sub>17</sub>Al<sub>12</sub> phase tends to be a successive net structure, which is adverse to the strength of the alloy if the net structure phase only consists of the  $\beta$ -Mg<sub>17</sub>Al<sub>12</sub> phase. Further proof provided by EDS results (see Figure 4c,f) indicates that the net structure changes from the  $\beta$ -Mg<sub>17</sub>Al<sub>12</sub> phase to the eutectic network together with  $\beta$ -Mg<sub>17</sub>Al<sub>12</sub> and Mg<sub>2</sub>Cu<sub>6</sub>Al<sub>5</sub> when Cu content varies from 1 to 3%, which is beneficial in terms of enhancing the strength of the alloy. However, when the addition of Cu increases to 5%, according to the EDS result in Figure 4i, the amount of the long-strip-shaped Mg<sub>2</sub>Cu<sub>6</sub>Al<sub>5</sub> phase continuously increases, and the continuous net structure is more remarkable and has adverse effects on the mechanical properties. This is because, when the amount of phase increases, the size of the aggregated phases is larger, and the eutectic network becomes continuous. These large networks separate the  $\alpha$ -Mg matrix, and the fragility of the large eutectic network makes the alloy premature fracture, exhibiting an obvious adverse effect on the mechanical properties. This experimental result indicated the Mg<sub>2</sub>Cu<sub>6</sub>Al<sub>5</sub> phase has a strengthening effect only when the amount of it is appropriate. Moreover, the Al<sub>4</sub>Cu<sub>9</sub> phase, which also possesses higher thermal stability, is mostly distributed along the grain boundaries, and a small amount of it is distributed inside the Mg grains. Moreover, with the increase in Cu content, the amount of Al<sub>4</sub>Cu<sub>9</sub> phase continuously increases; when the content of Cu is 3%, the amount and size of the Al<sub>4</sub>Cu<sub>9</sub> phase is appropriate. The distribution of the Al<sub>3</sub>Sm phase is also homogeneous. The Al<sub>3</sub>Sm phase is also mainly distributed in the Mg grains and the grain boundaries. The shape, size, and morphology of the Al<sub>4</sub>Cu<sub>9</sub> and Al<sub>3</sub>Sm phases are superior to those of the Mg<sub>2</sub>Cu<sub>6</sub>Al<sub>5</sub> phase. Therefore, the Al<sub>4</sub>Cu<sub>9</sub> phase and the Al<sub>3</sub>Sm phase are the main reinforced phases in the alloys.

Typical TEM bright field (BF) images and corresponding selected area electron diffraction (SAED) patterns for the eutectic phase are shown in Figure 5a,b, respectively. The Al<sub>3</sub>Sm phase can be observed in a TEM bright field (BF) image of the die-cast Mg-6Al-2Sm-3Cu alloy, and the corresponding selected area diffraction pattern confirms that it is an Al<sub>3</sub>Sm (tetragonal structure,  $a = 6.380$  nm,  $b = 6.380$  nm,  $c = 4.597$  nm) phase. Moreover, the Al<sub>3</sub>Sm phase possesses high thermal stability, which is beneficial for tensile strength at high temperature.

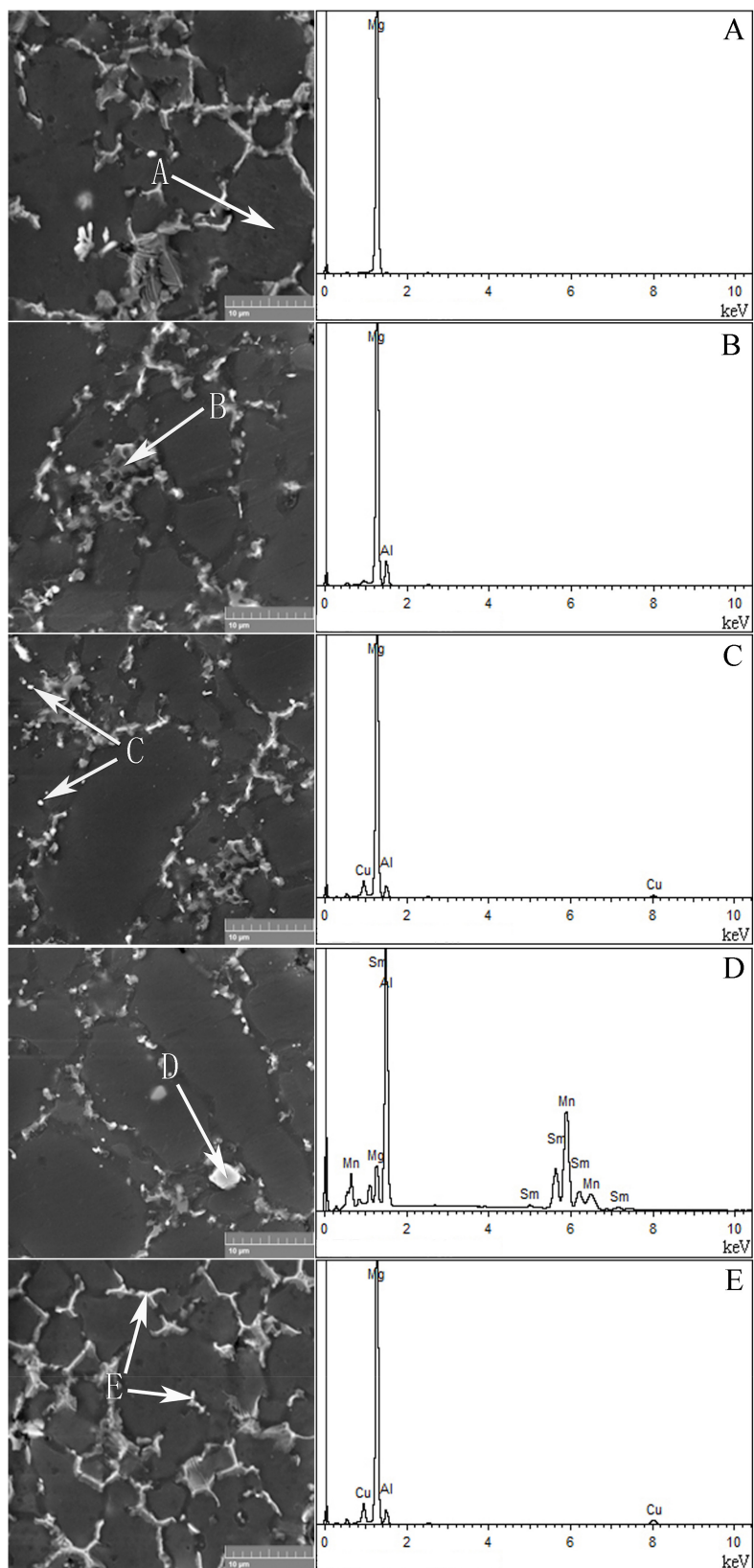
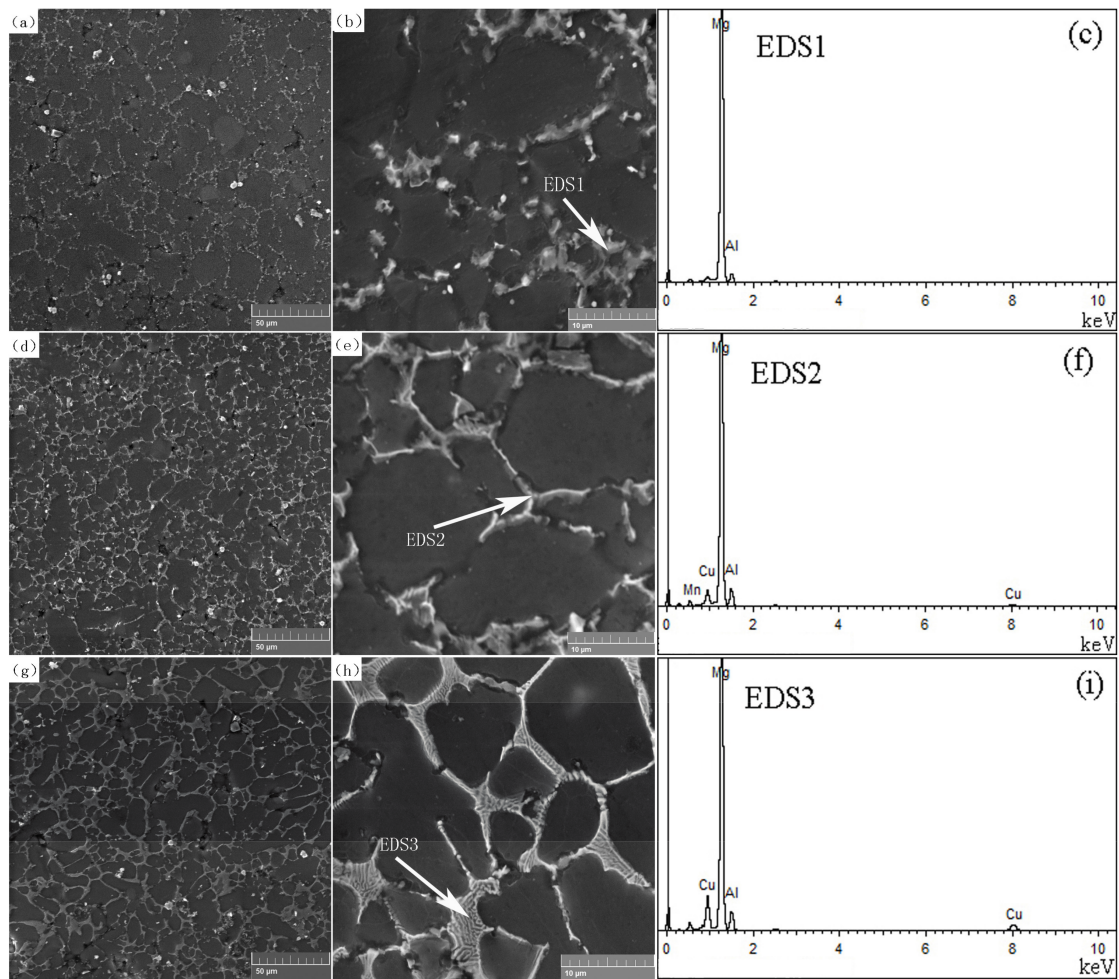
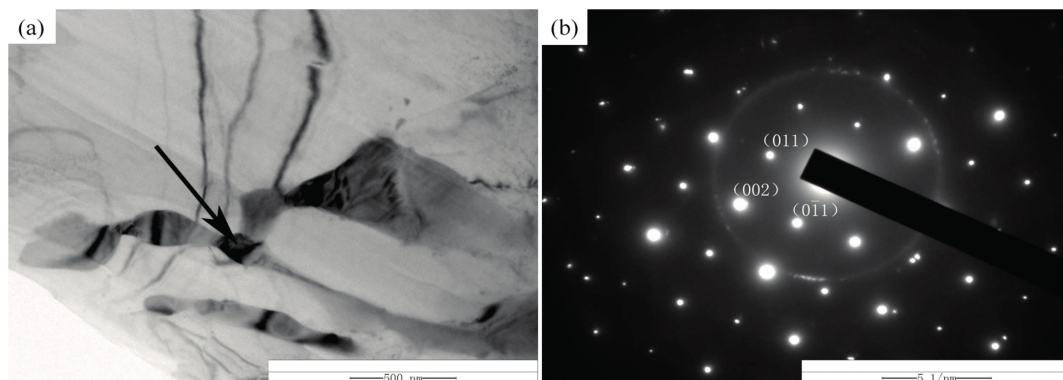


Figure 3. SEM morphologies of and EDS results of phases of die-cast alloys.



**Figure 4.** SEM morphologies (illustrations indicate local enlarged regions) and EDS results of the net structure of all die-cast alloys: (a–c) Mg-6Al-2Sm-1Cu; (d–f) Mg-6Al-2Sm-3Cu; (g–i) Mg-6Al-2Sm-5Cu.



**Figure 5.** Typical TEM bright field (BF) image of the die-cast Mg-6Al-2Sm-3Cu alloy and corresponding selected area electron diffraction (SAED) of the  $\text{Al}_3\text{Sm}$  phase.

### 3.2. The Mechanical Properties of Die-Cast Mg-6Al-2Sm-xCu Alloys ( $x = 1, 3, 5$ )

Table 1 shows the mechanical properties of the die-cast Mg-6Al-2Sm-xCu alloys ( $x = 1, 3, 5$ ) at room temperature. The ultimate tensile strengths and yield strength of the die-cast Mg-6Al-2Sm-1Cu, Mg-6Al-2Sm-3Cu and Mg-6Al-2Sm-5Cu alloys are 200 MPa, 250 MPa, and 214 MPa and 172 MPa, 186 MPa, and 182 MPa, respectively. Moreover, the elongation rates of the three alloys are 7.5%, 14.4%, and 5.7%, respectively. With the increase in Cu content, the ultimate tensile strength and yield strength of these experimental alloys increase firstly and then decrease, but the strength of the Mg-6Al-2Sm-5Cu alloy is still higher than that of the Mg-6Al-2Sm-1Cu alloy. The elongation rate of these alloys increases firstly and then decreases as Cu content increases. It can be concluded that, when the Cu content is 3%, the alloy shows the highest tensile strength and elongation rate among the three alloys. The enhancement of the alloy tensile strength is due to the fact that, during the solidification of the Mg-6Al-2Sm-xCu ( $x = 1, 3, 5$ ) alloys, Al is propitious to the solid-solution strengthening of the alloy [25], while Sm and Cu participate in the  $Al_3Sm$ ,  $Al_4Cu_9$ , and  $Mg_2Cu_6Al_5$  phases. The fine compounds mentioned above can constitute the reinforced phase of the alloy and impede the movement of dislocation and grain boundary sliding, so these strengthening effects help the alloy obtain a high strength. In addition, when the Cu content is increased to 3%, the microstructure is obviously refined. The alloy is capable of grain-refinement strengthening, solid-solution strengthening, precipitation strengthening, dispersion strengthening, and dislocation strengthening. Among these, the grain-refinement plays an important role on the mechanical properties of Mg alloys at room temperature, which has been confirmed by some experimental results [26–28]. It is believed that a fine grain size will increase the amount of grain boundary such that the dislocation movement is hindered, which in turn makes the alloy obtain a reinforcement effect. In addition, a fine grain size can help alloys obtain excellent plasticity [26–28]. In the present study, as Cu content increased, the grain size decreased first and then increased, which in turn made the elongation rate increase first and then decrease. Besides that, with the increase in Cu content, the amount of  $Al_4Cu_9$  and  $Mg_2Cu_6Al_5$  continuously increases. When the amount is greater, the size of the eutectic network is larger. The alloy will attain a premature failure (i.e., fracture) because the excessive large eutectic network increases the brittleness, and therefore, the elongation rate of the alloy decreases. This leads to a low ultimate tensile strength. Besides these, other strengthening effects, such as fine precipitates and particle dispersion, can be inferred, as for the alloy with 3% Cu. For these reasons, the tensile strength and elongation increase first and then decrease with the increase in Cu content.

**Table 1.** The mechanical properties of the die-cast Mg-6Al-2Sm-xCu alloys ( $x = 1, 3, 5$ ) at room temperature.

Experimental Alloy	Ultimate Tensile Strength (MPa)	Yield Strength (MPa)	Elongation Rate (%)
Mg-6Al-2Sm-1Cu	200	172	7.5
Mg-6Al-2Sm-3Cu	250	186	14.4
Mg-6Al-2Sm-5Cu	214	182	5.7

Table 2 shows the mechanical properties of the die-cast Mg-6Al-2Sm-xCu alloys ( $x = 1, 3, 5$ ) at 150 °C. The ultimate tensile strengths and yield strength of the die-cast Mg-6Al-2Sm-1Cu, Mg-6Al-2Sm-3Cu, and Mg-6Al-2Sm-5Cu alloys are 147 MPa, 178 MPa, and 159 MPa, and 126 MPa, 140 MPa, and 133 MPa, respectively. Moreover, the elongation rates of three corresponding alloys are 11.3%, 18.2%, and 8.6%, respectively. The tendency of the tensile strength at a high temperature is the same as that at room temperature. The experimental results under the condition of 150 °C also show the highest tensile strength and elongation when the Cu content is 3%. The tensile strength decreases as temperature is elevated from room temperature, but elongation increases. This is because the  $Mg_{17}Al_{12}$  phase is easy to soften at an elevated temperature [29], which means that the dislocation slip and grain boundary migration cannot be effectively controlled, i.e., the  $Mg_{17}Al_{12}$  phase is easily softened at elevated temperature decreases the strength of the alloy. As for the elongation rate, at 150 °C, increases

because, when the temperature is high, the single slip system evolves into multi-slip systems, which improves the slip orientations of the alloy samples. Therefore, the elongation, at a high temperature, increases, compared to that at room temperature. Under the condition of an elevated temperature, some phases with a high thermostability, such as  $\text{Al}_3\text{Sm}$  and  $\text{Al}_4\text{Cu}_9$ , still exist in alloys, and the morphology barely changes. These phases can still act as reinforcements and impede the movement of dislocation and grain boundary sliding, so, at a high temperature, mechanical properties can improve. However, this effect is not more powerful than that at room temperature. It is generally accepted that the strengthening mechanisms of the alloys at room temperature mainly include grain-refinement strengthening, solid-solution strengthening, precipitation strengthening, dispersion strengthening, and dislocation strengthening. In the present study, it is inferred that multiple strengthening effects may be responsible for the different mechanical properties at elevated temperatures.

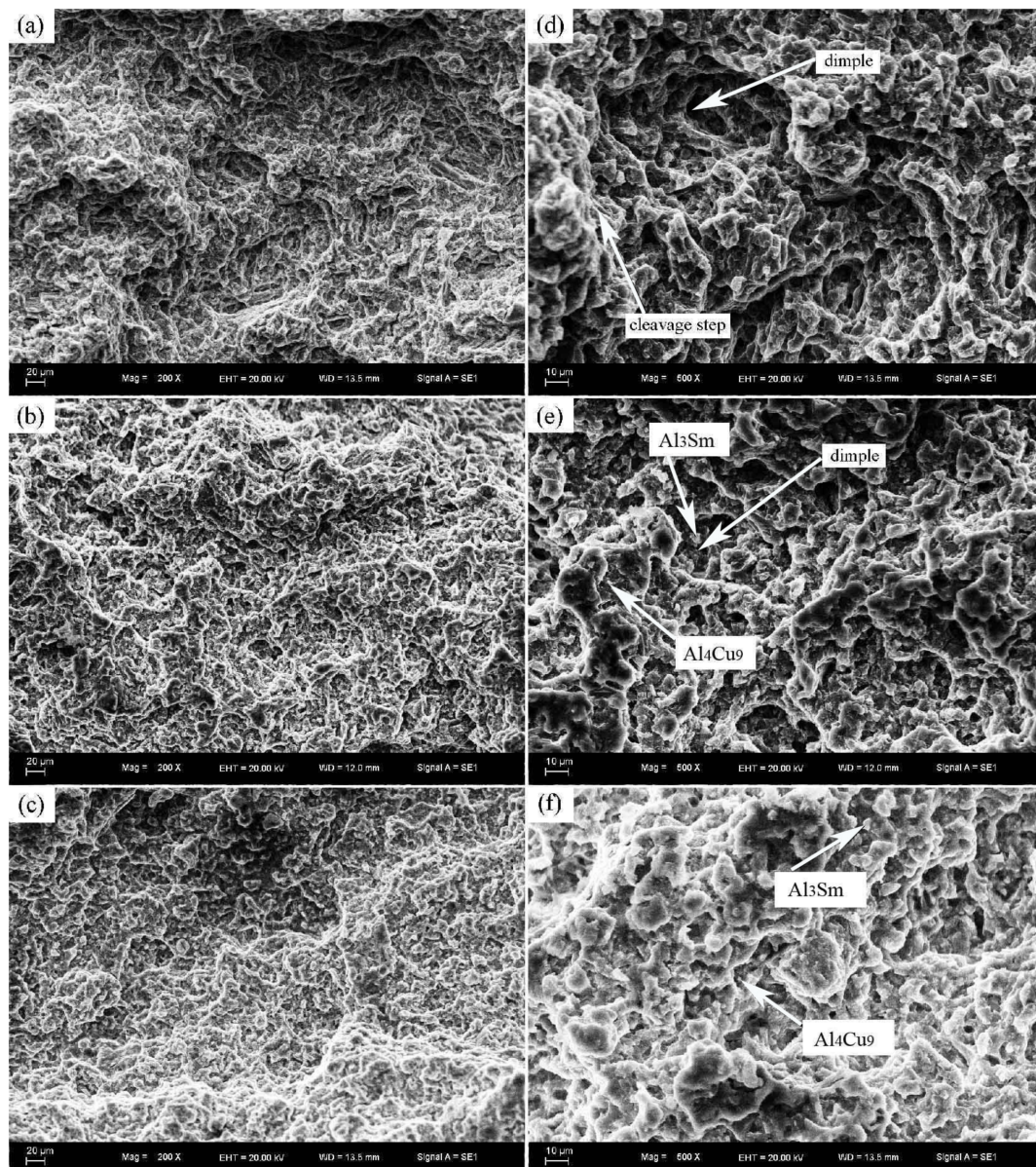
**Table 2.** The mechanical properties of the die-cast Mg-6Al-2Sm-xCu alloys ( $x = 1, 3, 5$ ) at high temperature (150 °C).

Experimental Alloy	Ultimate Tensile Strength (MPa)	Yield Strength (MPa)	Elongation Rate (%)
Mg-6Al-2Sm-1Cu	147	126	11.3
Mg-6Al-2Sm-3Cu	178	140	18.2
Mg-6Al-2Sm-5Cu	159	133	8.6

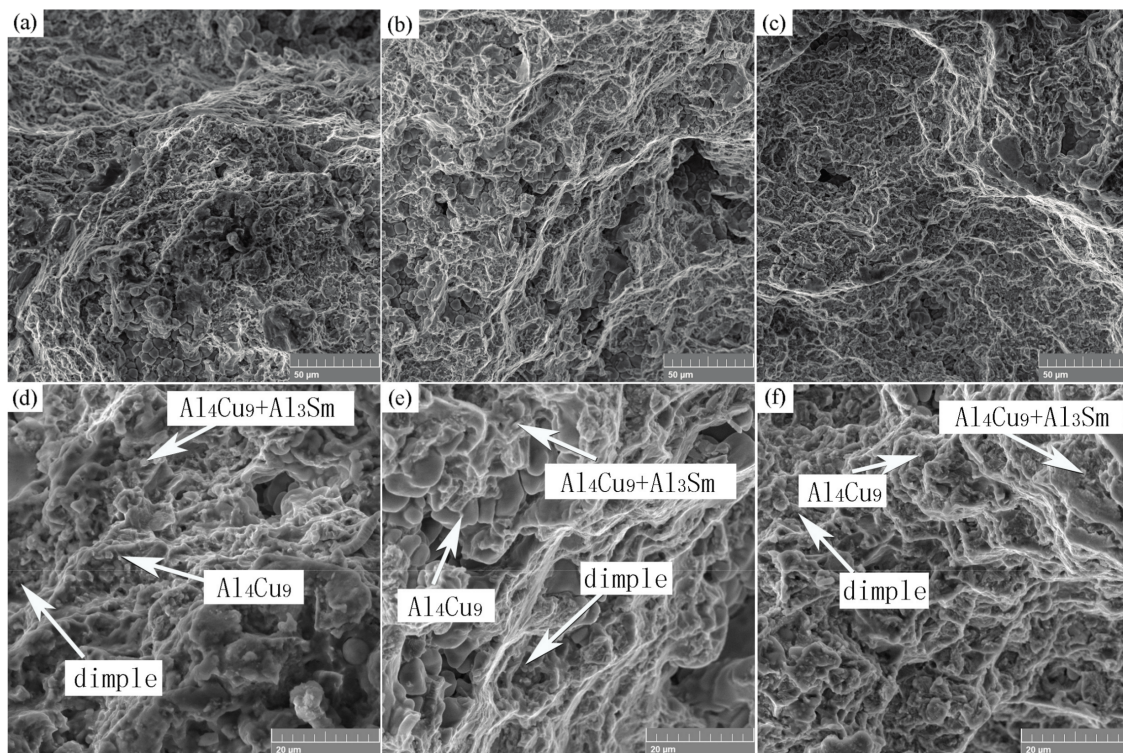
### 3.3. Fracture

Figure 6 shows the fracture surfaces of die-cast alloys after the tensile test at room temperature. All die-cast tensile fractures at room temperature show a complex mode. The wide and shallow dimples and cleavage steps can be seen on the fracture surface of the Mg-6Al-2Sm-1Cu alloy. Moreover, with an increase in Cu content, the amount of dimples increases firstly, and the dimples become deep, while the amount of cleavage steps decreases. When the content of Cu is increased to 5%, the dimples become unclear. This is consistent with the changes in tensile strength and elongation of the experimental alloys at room temperature. In addition, some particle phases and small block phases are distributed on the fracture surfaces of all alloys. These phases were shown to be the  $\text{Al}_4\text{Cu}_9$  phase and the  $\text{Al}_3\text{Sm}$  phase, according to EDS results shown in Figure 3. It can be observed that, when Cu content is increased to 3 wt. %, the amount of the  $\text{Al}_3\text{Sm}$  phase and the  $\text{Al}_4\text{Cu}_9$  phase is higher, and the distributions of these phases are homogeneous, which also confirms the high strength of the alloy.

Figure 7 shows SEM morphologies and corresponding local enlarged regions of the fracture surfaces of die-cast alloys after the tensile test at 150 °C. The variation in the tensile fracture at 150 °C is similar to that at room temperature. Under the condition of 150 °C, the die-cast tensile fractures of all alloys are more ductile, which is consistent with the variations in tensile strength and elongation of the experimental alloy at 150 °C. Compared to the fracture surface at room temperature, there are many more dimples at 150 °C. Moreover, the tear ridges on the fracture surface are pronounced at 150 °C. It can also be observed that some particles and small block phases also distribute on the fracture surfaces of all alloys; they are the  $\text{Al}_4\text{Cu}_9$  phase and compounds of  $\text{Al}_4\text{Cu}_9$  and  $\text{Al}_3\text{Sm}$ . These phases are similarly beneficial for the mechanical properties of the alloys.



**Figure 6.** SEM morphologies of tensile fractures of the die-cast alloys at room temperature (illustrations indicate local enlarged regions): (a,d) Mg-6Al-2Sm-1Cu; (b,e) Mg-6Al-2Sm-3Cu; (c,f) Mg-6Al-2Sm-5Cu.



**Figure 7.** SEM morphologies of tensile fractures of the die-cast alloys at 150 °C (illustrations indicate local enlarged regions): (a,d) Mg-6Al-2Sm-1Cu; (b,e) Mg-6Al-2Sm-3Cu; (c,f) Mg-6Al-2Sm-5Cu.

#### 4. Conclusions

(1) The grain size increases firstly and then decreases when the Cu content increases from 1% to 5%. When the Cu content is 3%, the grain size is fine, and the microstructure of the alloy is homogeneous. All die-cast Mg-6Al-2Sm- $x$ Cu ( $x = 1, 3$  and 5) alloys consist of  $\alpha$ -Mg matrix,  $\beta$ -Mg<sub>17</sub>Al<sub>12</sub>, Al<sub>4</sub>Cu<sub>9</sub>, Al<sub>3</sub>Sm, and Mg<sub>2</sub>Cu<sub>6</sub>Al<sub>5</sub>. The Al<sub>3</sub>Sm phase possesses a tetragonal structure.

(2) The ultimate tensile strength and yield strength of Mg-6Al-2Sm- $x$ Cu ( $x = 1, 3, 5$ ) alloys increases firstly and then decreases as Cu content increases at room temperature and an elevated temperature.

(3) All fracture surfaces at room temperature show a complex mode of brittle and ductile fracture. The fracture surfaces of all alloys at an elevated temperature show more ductile fracture.

**Acknowledgments:** This work was supported by The National Natural Science Foundation of China (No. 51201068).

**Author Contributions:** The experimental scheme was framed by Jiaan Liu. The tensile test at room temperature and elevated temperature were carried out by Chunxue Yang and Mengli Yang. The SEM, TEM and EDS characterization were performed by Chunxue Yang with the participation of Jiaan Liu. The XRD was analyzed by Mengli Yang. The manuscript was composed by Jiaan Liu and Chunxue Yang.

**Conflicts of Interest:** The authors declare no conflict of interest.

#### References

1. Aghion, E.; Bornfin, B. Magnesium alloys development towards the 21th century. *Mater. Sci. Forum* **2000**, *350*, 19–28. [[CrossRef](#)]
2. Zhang, J.; Zhang, L.; Leng, Z.; Liu, S.; Wu, R.; Zhang, M. Experimental study on strengthening of Mg-Li alloy by introducing long-period stacking ordered structure. *Scr. Mater.* **2013**, *68*, 675–678. [[CrossRef](#)]
3. Leng, Z.; Zhang, J.; Zhu, T.; Wu, R.; Zhang, M.; Liu, S.; Sun, J.; Zhang, L. Microstructure and mechanical properties of Mg-(6, 9) RY-4Zn alloys by extrusion and aging. *Mater. Des.* **2013**, *52*, 713–719. [[CrossRef](#)]

4. Li, K.; Li, Q.; Jing, X.; Chen, J.; Zhang, X. Effects of Sb, Sm, and Sn additions on the microstructure and mechanical properties of Mg-6Al-1.2Y-0.9Nd alloy. *Rare Met.* **2009**, *28*, 516–522. [[CrossRef](#)]
5. Zhang, J.; Xu, L.; Jiao, Y.; Xu, C.; Zhang, L.; Liu, S.; Meng, J.; Wu, R.; Zhang, M. Study of Mg-Ymm-Zn alloys with high-strength at elevated temperatures processed by water-cooled mold casting. *Mater. Sci. Eng. A* **2014**, *610*, 139–144. [[CrossRef](#)]
6. Zhang, L.; Zhang, J.; Xu, C.; Liu, S.; Jiao, Y.; Xu, L.; Wang, Y.; Meng, J.; Wu, R.; Zhang, M. Investigation of high-strength and superplastic Mg-Y-Gd-Zn alloy. *Mater. Des.* **2014**, *61*, 168–176. [[CrossRef](#)]
7. Liu, W.; Liu, Y.; Xiong, S. Influences of casting pressure conditions on the quality and properties of a magnesium cylinder head cover die casting. *J. Mater. Sci. Technol.* **2005**, *21*, 170–174.
8. Mehta, D.S.; Masood, S.H.; Song, W.Q. Investigation of wear properties of magnesium and aluminum alloys for automotive applications. *J. Mater. Process. Technol.* **2004**, *155*, 1526–1531. [[CrossRef](#)]
9. Zhang, L.; Zhang, J.; Xu, C.; Jing, Y.; Zhuang, J.; Wu, R.; Zhang, M. Formation of stacking faults for improving the performance of biodegradable Mg-Ho-Zn alloy. *Mater. Lett.* **2014**, *133*, 158–162. [[CrossRef](#)]
10. Leng, Z.; Zhang, J.; Cui, C.; Sun, J.; Liu, S.; Wu, R.; Zhang, M. Compression properties at different loading directions of as-extruded Mg-9RY-4Zn(RY: Y-rich misch metal) alloy with long period stacking ordered phase. *Mater. Des.* **2013**, *51*, 561–566. [[CrossRef](#)]
11. Chen, Y.; Jin, L.; Fang, D.; Song, Y.; Ye, R. Effects of calcium, samarium addition on microstructure and mechanical properties of AZ61 magnesium alloy. *J. Rare Earth* **2015**, *33*, 86–92. [[CrossRef](#)]
12. Leng, Z.; Zhang, J.; Yin, T.; Zhang, L.; Liu, S.; Zhang, M.; Wu, R. Microstructure and mechanical properties of Mg-9RY-4Cu alloy with long period stacking ordered phase. *Mater. Sci. Eng. A* **2013**, *580*, 196–201. [[CrossRef](#)]
13. Wang, J.; Wang, L.; Wu, Y.; Wang, L. Effects of samarium on microstructures and tensile properties of Mg-5Al-0.3Mn alloy. *Mater. Sci. Eng. A* **2011**, *528*, 4115–4119. [[CrossRef](#)]
14. Zhang, J.; Liu, S.; Leng, Z.; Liu, X.; Niu, Z.; Zhang, M.; Wu, R. Structure stability and mechanical properties of high-pressure die-cast Mg-Al-La-Y-based alloy. *Mater. Sci. Eng. A* **2012**, *531*, 70–75. [[CrossRef](#)]
15. Zhang, J.; Liu, S.; Leng, Z.; Zhang, M.; Meng, J.; Wu, R. Structure stability and mechanical properties of high-pressure die-cast Mg-Al-Ce-Y-based alloy. *Trans. Nonferr. Met. Soc.* **2012**, *22*, 262–267. [[CrossRef](#)]
16. Wang, J.; Peng, Q.; Wu, Y.; Wang, L. Microstructure and mechanical properties of Mg-6Al-4RE-0.4Mn alloy. *Trans. Nonferr. Met. Soc.* **2006**, *16*, s1703–s1707.
17. Tong, G.; Liu, H.; Liu, Y. Effect of rare earth additions on microstructure and mechanical properties of AZ91 magnesium alloys. *Trans. Nonferr. Met. Soc.* **2010**, *20*, s336–s340. [[CrossRef](#)]
18. Zhang, J.; Yu, P.; Liu, K.; Fang, D.; Tang, D.; Meng, J. Effect of substituting cerium-rich mischmetal with lanthanum on microstructure and mechanical properties of die-cast Mg-Al-RE alloys. *Mater. Des.* **2009**, *30*, 2372–2378. [[CrossRef](#)]
19. Luo, A.A. Recent magnesium alloy development for elevated temperature applications. *Int. Mater. Rev.* **2004**, *49*, 13–30. [[CrossRef](#)]
20. Pekguleryuz, M.O.; Kaya, A.A. Creep resistant magnesium alloys for powertrain applications. *Adv. Eng. Mater.* **2003**, *5*, 866–878. [[CrossRef](#)]
21. Zhang, L.; Zhang, J.; Leng, Z.; Liu, S.; Yang, Q.; Wu, R.; Zhang, M. Microstructure and mechanical properties of high-performance Mg-Y-Er-Zn extruded alloy. *Mater. Des.* **2014**, *54*, 256–263. [[CrossRef](#)]
22. Son, H.T.; Lee, J.S.; Kim, D.G.; Yoshimi, K.; Maruyama, K. Effects of samarium (Sm) additions on the microstructure and mechanical properties of as-cast and hot-extruded Mg-5 wt. % Al-3 wt. % Ca-based alloys. *J. Alloys Compd.* **2009**, *473*, 446–452. [[CrossRef](#)]
23. Xia, X.; Zhang, K.; Li, X.; Ma, M.; Li, Y. Microstructure and texture of coarse-grained Mg-Gd-Y-Nd-Zr alloy after hot compression. *Mater. Des.* **2013**, *44*, 521–527. [[CrossRef](#)]
24. Zheng, J.; Wang, Q.; Jin, Z.; Peng, T. Effect of Sm on the microstructure, mechanical properties and creep behavior of Mg-0.5Zn-0.4Zr based alloys. *Mater. Sci. Eng. A* **2010**, *527*, 1677–1685. [[CrossRef](#)]
25. Huang, Z.; Qi, W.; Xu, J.; Cai, C. Microstructures and mechanical properties of Mg-Al-Sm series heat-resistant magnesium alloys. *Trans. Nonferr. Met. Soc.* **2015**, *25*, 22–29. [[CrossRef](#)]
26. Prabhu, T.R. Effect of synthetic graphite and activated charcoal addition on the mechanical, microstructure and wear properties of AZ81 Mg alloys. *J. Mater. Res. Technol.* **2016**, *5*, 259–267. [[CrossRef](#)]
27. Pranke, K.; Eigenfeld, K. About ultrasonic melt treatment during solidification and its influence on grain size and mechanical properties of magnesium alloy AZ 91. *Mater. Sci. Forum* **2010**, *649*, 295–300. [[CrossRef](#)]

28. Wang, Y.N.; Lee, C.J.; Huang, C.C.; Lin, H.K.; Huang, J.C. Influence from extrusion parameters on high strain rate and low temperature superplasticity of AZ series Mg-based alloys. *Mater. Sci. Forum* **2003**, *426*, 2655–2660. [[CrossRef](#)]
29. Jiao, Y.; Zhang, J.; He, L.; Zhang, M.; Jiang, F.; Wang, W.; Han, L.; Xu, L.; Wu, R. Al-RE Intermetallic Phase Stability and Effects on Corrosion Behavior in Cold-Chamber HPDC AE44 Alloy. *Adv. Eng. Mater.* **2016**, *18*, 148–155. [[CrossRef](#)]



© 2017 by the authors. Licensee MDPI, Basel, Switzerland. This article is an open access article distributed under the terms and conditions of the Creative Commons Attribution (CC BY) license (<http://creativecommons.org/licenses/by/4.0/>).